J Mater Sci (2009) 44:4577–4586
DOI 10.1007/s10853-009-3696-0

Comparison about effects of Ce, Sn and Gd additions on as-cast microstructure and mechanical properties of Mg–3.8Zn–2.2Ca (wt%) magnesium alloy

Mingbo Yang · Liang Cheng · Fusheng Pan

Received: 31 March 2009 / Accepted: 16 June 2009 / Published online: 2 July 2009

Abstract In this paper, the effects of Ce, Sn and Gd additions on the as-cast microstructure and mechanical properties of Mg–3.8Zn–2.2Ca (wt%) magnesium alloy are investigated and compared. The results indicate that adding 1.0 wt% Ce, 1.0 wt% Sn or 1.0 wt% Gd can effectively refine the grains of the Mg–3.8Zn–2.2Ca alloy, and the refinement efficiency of Ce addition is relatively high, followed by the additions of Sn and Gd, respectively. Accordingly, the tensile properties of the as-cast Mg–3.8Zn–2.2Ca alloy are improved by the additions of Ce, Sn or Gd, with the improvement resulting from the Ce addition being best and followed by the additions of Sn and Gd, respectively. In addition, adding 1.0 wt% Ce, 1.0 wt% Sn or 1.0 wt% Gd to the Mg–3.8Zn–2.2Ca alloy can also improve the creep properties of the as-cast alloy. Among the Ce-, Sn- and Gd-containing alloys, the creep properties of the Sn- and Gd-containing alloys are similar but lower than that of the Ce-containing alloy.

Introduction

Magnesium alloys are the lightest structural alloys commercially available and have great potential for applications in automotive, aerospace and other industries. At present, the widely used magnesium alloys are from the Mg–Al series alloys, such as AZ91 and AM60 alloys, but their structural applications are limited by a poor strength and corrosion resistance at elevated temperatures [1]. Therefore, improving the strength and the corrosion and creep resistance at elevated temperatures has become a critical issue for possible application of magnesium alloys in hot components. In recent years, efforts have been made to develop new high-strength and creep-resistant magnesium alloys based on the Mg–Zn–Ca system for the following reasons [2–10]: (1) Zn can enhance the age-hardening response and improve the castability, and has several stable intermetallics with Mg; (2) Ca not only behaves as a grain refiner but also can improve the corrosion resistance and form a stable Mg_2Ca compound with Mg; (3) Zn and Ca together with Mg may form the stable intermetallic compound $Ca_2Mg_6Zn_3$. To date, some mechanical properties have been reported for the Mg–Zn–Ca alloys. For example, Gao et al. [11] reported that the tensile and creep properties of Mg–1Zn–1Ca–0.6Zr (wt%) alloy are superior to magnesium alloy AZ91, and the addition of 1 wt% Nd to this alloy leads to further improvements in yield strength and creep resistance. Somekawa and Mukai [12] found that the as-extruded Mg–1.8Zn–0.3Ca (at%) alloy shows a good balance of yield strength and plane-strain fracture toughness, and these are higher than those of conventional wrought magnesium alloys. Levi et al. [4] reported that the Mg–3.2Zn–1.6Ca (wt%) alloy can show a clear age-hardening response during an aging treatment as well as during exposure to elevated temperatures. Ortega et al. [13] investigated the tensile fracture behavior of the age-hardened Mg–1Zn–1Ca alloy, and found the precipitates formed in the aged alloy are beneficial to improve the mechanical properties of the alloy at elevated temperatures. In addition, some investigations about the microstructure and properties of rapidly solidified Mg–Zn–Ca alloys have been reported [14–17].

M. Yang (✉) · L. Cheng
Materials Science and Engineering College, Chongqing University of Technology, Chongqing 400050, China
e-mail: yangmingbo@cqut.edu.cn

M. Yang · F. Pan
National Engineering Research Center for Magnesium Alloys, Chongqing University, Chongqing 400030, China

Though the above-mentioned studies have been carried out to develop high-strength and creep-resistant Mg–Zn–Ca magnesium alloys, these works mainly focus on the microstructural characterization and age-hardening behavior of a limited number of Mg–Zn–Ca alloys. The investigations of the tensile and creep properties of Mg–Zn–Ca alloys and the potential for further improvement in strength and creep performance via further alloying/microalloying additions are very scarce in the literature. For these reasons, the present work investigates and compares the influence of Ce, Sn and Gd additions, all of which have been successfully used to improve the mechanical properties of other magnesium alloy systems [18–24], on the as-cast microstructure and mechanical properties of Mg–3.8Zn–2.2Ca (wt%) alloy (previously reported by Qian and Das [25]).

Fig. 1 Image for the pouring casting of the experimental alloys

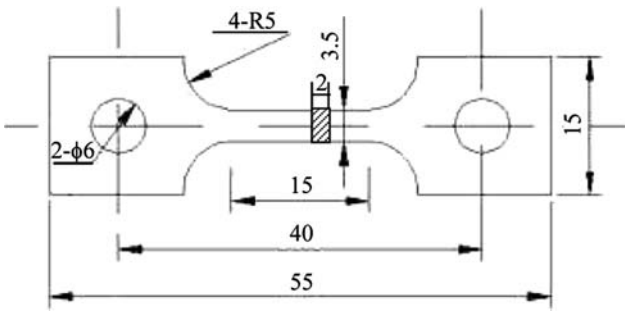

Fig. 2 Size of the samples used for tensile and creep tests (in mm)

Experimental procedures

The Mg–3.8Zn–2.2Ca alloys containing Ce, Sn or Gd were prepared from pure Mg, Zn and Sn (>99.9 wt%), and Mg–19wt%Ca, Mg–29wt%Ce and Mg–25wt%Gd master alloys. The experimental alloys were melted in a resistance furnace and protected by a flux addition. After the Ce, Sn and Gd were added to the melt at 740 °C, the melt was homogenized by mechanical stirring and held at 740 °C for 20 min before pouring into a permanent mould which was coated and preheated to 150 °C in order to obtain a casting as shown in Fig. 1. The tensile and creep specimens as shown in Fig. 2 were fabricated by linear cutting from the casting. For comparison, the ternary Mg–3.8Zn–2.2Ca alloy was also cast, machined into the same dimensions and tested under the same conditions as the above-mentioned samples. Furthermore, specimens were subjected to an annealing treatment (300 °C/12 h + 450 °C/12 h, water cooled) in order to clearly reveal the grain boundaries. Table 1 lists the actual chemical compositions of the experimental alloys, which were inspected by inductively coupled plasma spectroscopy.

Table 1 Actual compositions of experimental alloys (wt%)

Experimental alloys	Zn	Ca	Ce	Sn	Gd	Mg
1# alloy (Mg–3.8Zn–2.2Ca)	3.69	2.05	–	–	–	Bal.
2# alloy (Mg–3.8Zn–2.2Ca–1.0Ce)	3.71	2.11	0.89	–	–	Bal.
3# alloy (Mg–3.8Zn–2.2Ca–1.0Sn)	3.66	2.12	–	0.90	–	Bal.
4# alloy (Mg–3.8Zn–2.2Ca–1.0Gd)	3.67	2.08	–		0.88	Bal.

In order to analyze the solidification behavior of the experimental alloys, differential scanning calorimetry (DSC) was carried out using a NETZSCH STA 449C system. Samples weighing approximately 30 mg were heated in a flowing argon atmosphere from 30 to 700 °C for 5 min before being cooled down to 100 °C. The heating and cooling curves were recorded at a controlling speed of 15 °C/min.

The as-cast and heat-treated samples were etched with an 8% nitric acid distilled water solution, and then examined by using an Olympus optical microscope and JEOL/JSM-6460LV scanning electron microscope (SEM) operated at 20 kV. The grain size was measured by the standard linear intercept method using an Olympus stereomicroscope. The phases in the experimental alloys were analyzed by D/Max-1200X type X-ray diffraction (XRD) operated at 40 kV and 30 mA.

The tensile properties of the as-cast experimental alloys at room temperature and 150 °C were determined from a stress–strain curve. The tensile specimens tested at 150 °C were heated in a bisected resistance furnace with the temperature controlled to within ±2 °C and protected by CO_2 atmosphere. The ultimate tensile strength (UTS), 0.2% yield strength (YS) and elongation to failure (Elong.) were obtained based on the average of three tests. The constant-load tensile creep tests of the as-cast experimental alloys were performed at 150 °C and 50 MPa for 100 h.

Creep specimens were heated in a bisected resistance furnace with the temperature controlled to within ±2 °C and protected by CO_2 atmosphere. Creep strain was measured by extensometers which were attached directly to the surfaces of specimens. The total creep strain and minimum creep rates of the experimental alloys were respectively measured from each elongation versus time curve.

Results and discussion

Comparison of as-cast microstructure

Figure 3 shows the XRD results of the as-cast alloys. It is found from Fig. 3 that the ternary Mg–3.8Zn–2.2Ca alloy is mainly composed of α-Mg, Mg_2Ca and $Ca_2Mg_6Zn_3$ phases. Furthermore, it is found that the additions of 1.0 wt% Ce, 1.0 wt% Sn and 1.0 wt% Gd to the Mg–3.8Zn–2.2Ca alloy lead to the formation of the extra phases of $Mg_{12}Ce$, CaMgSn and Mg_5Gd, respectively. The XRD results may be further confirmed by the DSC results of the as-cast experimental alloys. Figure 4 shows the DSC cooling curves of these alloys. All the curves are similar, with three main peaks at about 610, 430 and 400 °C, respectively, corresponding to the α-Mg matrix solidification and second phase transformations. Based on the Mg–Zn–Ca ternary phase diagram and combined with the previous investigations [4, 26, 27], it is inferred that during the solidification of the experimental alloys the primary α-Mg phase first nucleates and grows until the temperature falls to about 430 °C where a binary eutectic reaction (L → α-Mg + Mg_2Ca) occurs and then at about 400 °C a second binary eutectic reaction (L → α-Mg + $Ca_2Mg_6Zn_3$) occurs rather than a ternary eutectic reaction (L → α-Mg + Mg_2Ca + $Ca_2Mg_6Zn_3$) since the Zn/Ca atomic ratio of the residual liquid is more than 1.2 [27]. Accordingly, the final as-cast microstructures of the experimental alloys mainly consist of α-Mg, Mg_2Ca and $Ca_2Mg_6Zn_3$ phases. Furthermore, it is found from Fig. 4 that a peak at about 505 °C is uniquely observed in the cooling curve of the Sn-containing alloy. This possibly corresponds to the formation of the CaMgSn phase, which is a typical precipitate in the Mg–Sn–Ca system alloys and has been described in detail in Refs. [18, 28].

Figure 5 shows the as-cast microstructures of the experimental alloys. It is observed that the primary α-Mg phases in the alloys are dendritic in nature, and the dendrite

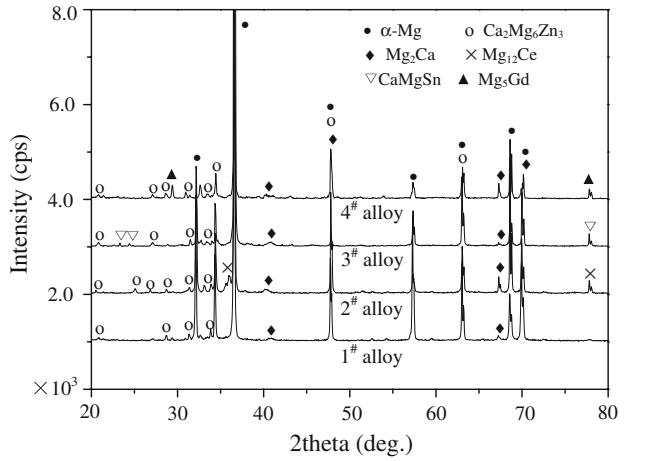

Fig. 3 XRD results of the as-cast experimental alloys

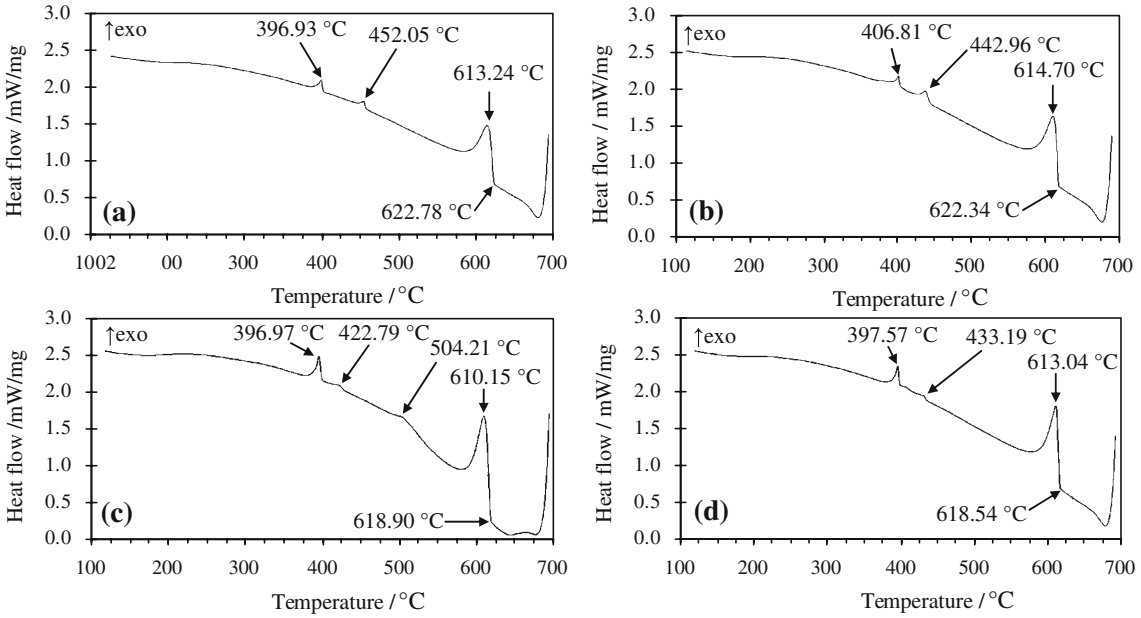

Fig. 4 DSC cooling curves of the as-cast experimental alloys: **a** 1# alloy; **b** 2# alloy; **c** 3# alloy; **d** 4# alloy

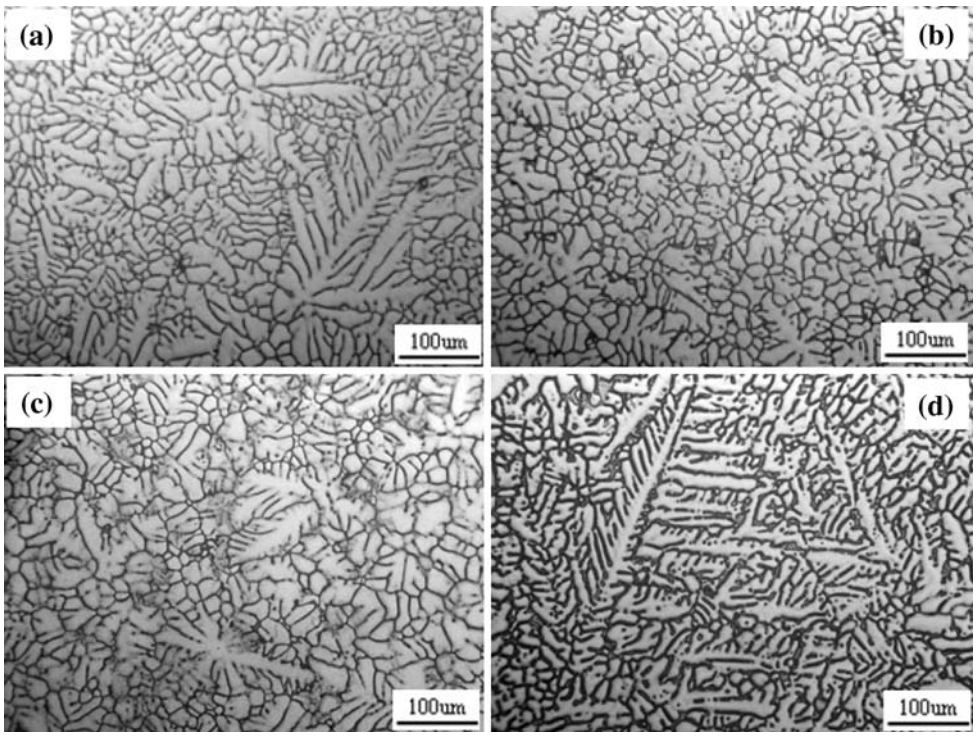

Fig. 5 Optical images of the as-cast experimental alloys: **a** 1# alloy; **b** 2# alloy; **c** 3# alloy; **d** 4# alloy

arm spacing and grain size of the ternary Mg–3.8Zn–2.2Ca alloy are relatively large. However, with additions of 1.0 wt% Ce, 1.0 wt% Sn and 1.0 wt% Gd, not only do the dendrite arm spacing and grain size of the alloys decrease, but there is a trend toward a more equiaxed structure especially in the Ce- and Sn-containing alloys. Figure 6 shows the solutionized microstructures of the experimental alloys. It is observed that these microstructures comprise α-Mg grains and some undissolved intermetallic particles both inside the grains and between the grains. Furthermore, it is found from Fig. 6 that the α-Mg grains in the Ce-, Sn- and Gd-containing Mg–3.8Zn–2.2Ca alloys are finer than those in the Mg–3.8Zn–2.2Ca alloy. As shown in Fig. 6a, the α-Mg grains in the Mg–3.8Zn–2.2Ca alloy have an average size of 234 μm. However, as shown in Fig. 6b and c, the additions of 1.0 wt% Ce and 1.0 wt% Sn to this alloy lead to significant grain refinement and a more uniform grain size, typically 71 and 82 μm in average size. Compared with the additions of 1.0 wt% Ce and 1.0 wt% Sn, the grain refinement efficiency of adding 1.0 wt% Gd is relatively poor (132 μm in average size). In addition, the obvious equiaxed trend observed in Fig. 5 for the primary α-Mg phases in the Ce- and Sn-containing alloys are also further confirmed in Fig. 6b and c. The above-mentioned results indicate that adding 1.0 wt% Ce, 1.0 wt% Sn and 1.0 wt% Gd to the Mg–3.8Zn–2.2Ca alloy can refine the grains of the alloy, and the refinement efficiency of the Ce addition is higher than that of the Sn and Gd additions.

Figure 7 shows the SEM images of the as-cast microstructures, which are comprised of α-Mg grains and a continuous and sparse distribution of intermetallic particles along grain boundaries and within grains, respectively. Combining the XRD and EDS results, the intermetallic compounds are identified as $Ca_2Mg_6Zn_3$, Mg_2Ca, $Mg_{12}Ce$ and Mg_5Gd phases mainly distributed at the grain boundaries, and small amounts of $Ca_2Mg_6Zn_3$ present within grains. Furthermore, it is observed from Fig. 7 that parts of the continuous $Ca_2Mg_6Zn_3$ ternary phases are interrupted by the Mg_2Ca phases, which was also reported for other Mg–Zn–Ca alloys [4, 27]. Moreover, it is shown in Fig. 7b that adding 1.0 wt% Ce to the Mg–3.8Zn–2.2Ca alloy causes an interesting microstructural change to the eutectic. The morphology of $Ca_2Mg_6Zn_3$ changes, in part, from initial continuous blocks to fine particles. However, the reason for the morphologic change of $Ca_2Mg_6Zn_3$ phases in the Ce-containing Mg–3.8Zn–2.2Ca alloy is not clear and further investigation needs to be considered. With the addition of Sn, the $Ca_2Mg_6Zn_3$ phase seems to become coarser and more continuous in nature, and the CaMgSn phase, with a rod- and/or needle-like morphology, is found to mainly distribute at grain boundaries and within grains.

Comparison of mechanical properties

The tensile properties of the as-cast experimental alloys, including ultimate tensile strength (UTS), 0.2% yield

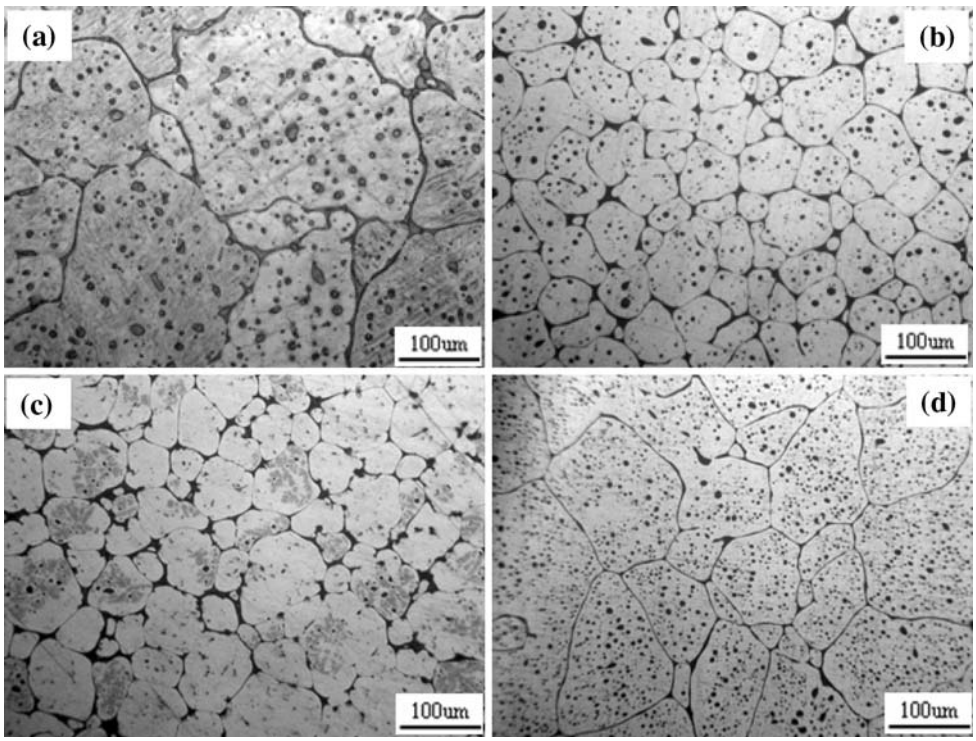

Fig. 6 Optical images of the solutionized experimental alloys: **a** 1# alloy; **b** 2# alloy; **c** 3# alloy; **d** 4# alloy

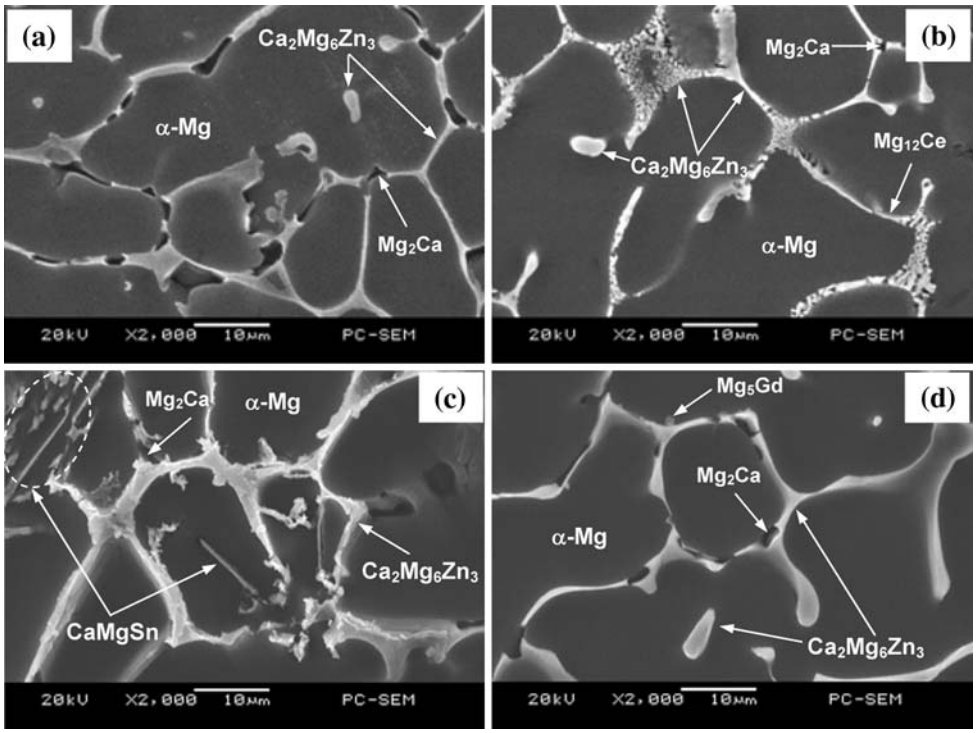

Fig. 7 SEM images of the as-cast experimental alloys: **a** 1# alloy; **b** 2# alloy; **c** 3# alloy; **d** 4# alloy

strength (YS) and elongation (Elong.), are listed in Table 2. It is observed that the tensile properties of the quarternary alloys at room temperature and 150 °C are higher than those of the base ternary alloy, indicating that adding 1.0 wt% Ce, 1.0 wt% Sn and 1.0 wt% Gd to the Mg–3.8Zn–2.2Ca alloy can improve both the tensile strength and elongation of the alloy. This situation is possibly related to the grain refinement of the Ce-, Sn- and

Table 2 Tensile properties of the as-cast experimental alloys at room temperature and 150 °C

Experimental alloys	Room temperature			150 °C		
	UTS (MPa)	YS (MPa)	Elong. (%)	UTS (MPa)	YS (MPa)	Elong. (%)
1# alloy	123.8 (4.1)	96.7 (2.9)	2.4 (0.21)	110.9 (3.3)	87.0 (1.6)	5.8 (1.01)
2# alloy	146.1 (3.8)	119.2 (2.7)	3.5 (0.15)	132.6 (2.9)	108.7 (1.4)	9.9 (1.12)
3# alloy	134.3 (2.9)	117.8 (3.2)	3.0 (0.17)	121.2 (1.8)	104.4 (2.0)	7.8 (0.98)
4# alloy	130.6 (3.1)	114.2 (2.1)	2.9 (0.15)	117.5 (2.0)	102.9 (2.2)	7.1 (1.02)

The data in the bracket is the standard error

Gd-containing Mg–3.8Zn–2.2Ca alloys. Furthermore, it is observed from Table 2 that among the Ce-, Sn- and Gd-containing Mg–3.8Zn–2.2Ca alloys the tensile properties of the Ce-containing alloy at room temperature and 150 °C are the highest, followed by the Sn- and Gd-containing alloys, respectively, which is possibly related to the different grain refinement efficiencies of Ce, Sn and Gd additions in Mg–3.8Zn–2.2Ca alloy. In addition, although the Sn addition exhibits similar grain refinement efficiency in Mg–3.8Zn–2.2Ca alloy with the Ce addition, the ultimate tensile strength and elongation of Sn-containing alloy at room temperature and 150 °C are relatively lower than those of the Ce-containing alloy. As shown in Fig. 7, the $Ca_2Mg_6Zn_3$ phases in the Sn-containing Mg–3.8Zn–2.2Ca alloy seem to be more coarse and continuous than those in the other Mg–3.8Zn–2.2Ca alloys, and the CaMgSn phases

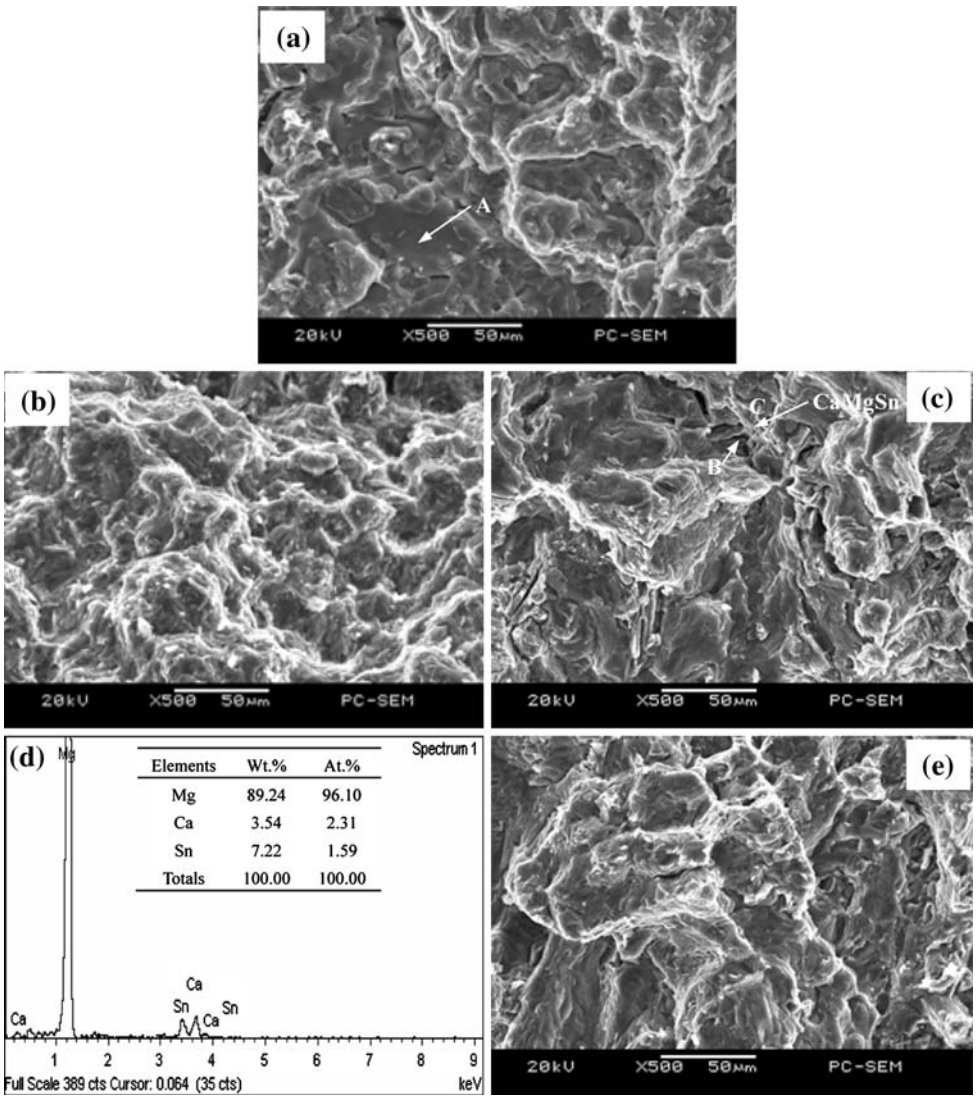

Fig. 8 SEM images of tensile fractographs for the as-cast experimental alloys tested at room temperature: **a** 1# alloy; **b** 2# alloy; **c** 3# alloy; **d** EDS results of position C in **c**; **e** 4# alloy

at grain boundaries and within grains in the alloy mainly exhibit a rod- and/or needle-like morphology. Therefore, it is inferred that the difference of Sn- and Ce-containing Mg–3.8Zn–2.2Ca alloys in the tensile properties is possibly related to the CaMgSn and $Ca_2Mg_6Zn_3$ phases in the Sn-containing Mg–3.8Zn–2.2Ca alloy. Actually, the above-mentioned results may be further confirmed from Figs. 8, 9, and 10. As shown in Fig. 8, a number of cleavage planes and steps are present, and some minute lacerated ridges can also be observed in the localized areas of the tensile fracture surfaces, indicating that all the tensile fracture surfaces have mixed characteristics of cleavage and quasi-cleavage fractures. Therefore, it is inferred that the addition of 1.0 wt% Ce, 1.0 wt% Sn or 1.0 wt% Gd to the Mg–3.8Zn–2.2Ca alloy does not significantly change the fracture mode. However, the fracture surface of the Mg–3.8Zn–2.2Ca alloy exhibits relatively large cleavage-type facets (arrow 'A' in Fig. 8a). On the other hand, the cleavage-type facets in the fracture surfaces of Ce-, Sn- and Gd-containing Mg–3.8Zn–2.2Ca alloys especially the Ce-containing alloy are relatively small. Furthermore, it is observed that the fracture surface of Sn-containing Mg–3.8Zn–2.2Ca alloy contains some small cracks possibly associated with the CaMgSn phase (arrows 'B' in Fig. 8c). In addition, it is also observed from Figs. 9 and 10 that, although the tensile rupture of the as-cast experimental alloys occurs along inter-granular boundary, the cracks seem to easily extend along the interfaces between continuous $Ca_2Mg_6Zn_3$, needle-like CaMgSn particles and α-Mg matrix for 1#, 3# and/or 4# alloys (arrow 'A' in Fig. 9a, c, d). It is well known that the initiation of microcracks can be greatly influenced by the presence and nature of the second phase. A common situation is for the particle to be cracked during deformation. Resistance to cracking is improved if the particle is well bonded to the matrix. The dispersion of second phase particles is easily cut by the dislocations, then there will be planar slip and relatively large dislocation pile-ups will occur. This will lead to high stress, easy initiation of microcracks and brittle behavior [29]. Small and spherical particles are more resistant to cracking. Obviously, the continuous $Ca_2Mg_6Zn_3$ and/or needle-like CaMgSn particles in the 1#, 3# and 4# alloys are easily fractured. However, this needs further confirmation.

Figure 11 shows the creep curves of the as-cast experimental alloys at 150 °C and 50 MPa. The total creep strain and minimum creep rate for 100 h are summarized in Table 3. As reference, the total creep strain and minimum creep rate of the AE42 and AZ91 alloys at 150 °C and 50 MPa for 100 h are also listed in Table 3. It is found from Table 3 that the Ce-, Sn- and Gd-containing Mg–3.8Zn–2.2Ca alloys have higher creep properties than the AZ91 alloy while the creep properties of all the as-cast experimental alloys are lower than those of the AE42 alloy. Furthermore, it is found from Fig. 11 and Table 3 that adding 1.0 wt% Ce, 1.0 wt% Sn and 1.0 wt% Gd to the Mg–3.8Zn–2.2Ca alloy can improve the creep properties of the alloy. Since the creep properties of magnesium alloys are mainly related to the structure stability at high temperatures, the

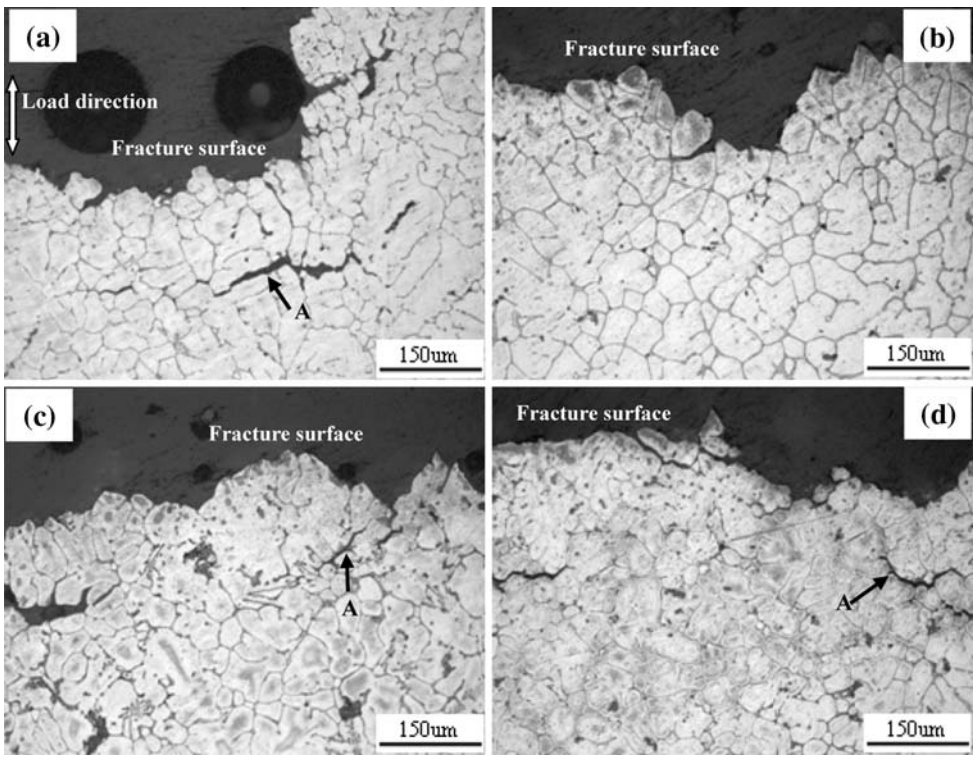

Fig. 9 Optical images of longitudinal sections for the as-cast experimental alloys failed in tensile test at room temperature: **a** 1# alloy; **b** 2# alloy; **c** 3# alloy; **d** 4# alloy

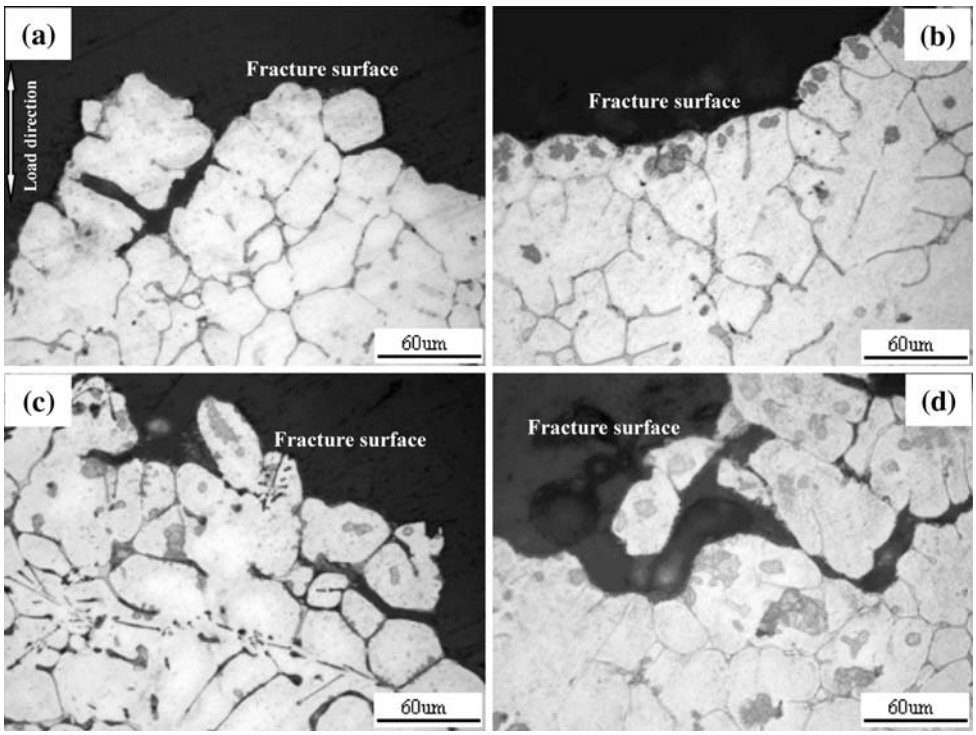

Fig. 10 Optical images of longitudinal sections for the as-cast experimental alloys failed in tensile test at 150 °C: **a** 1# alloy; **b** 2# alloy; **c** 3# alloy; **d** 4# alloy

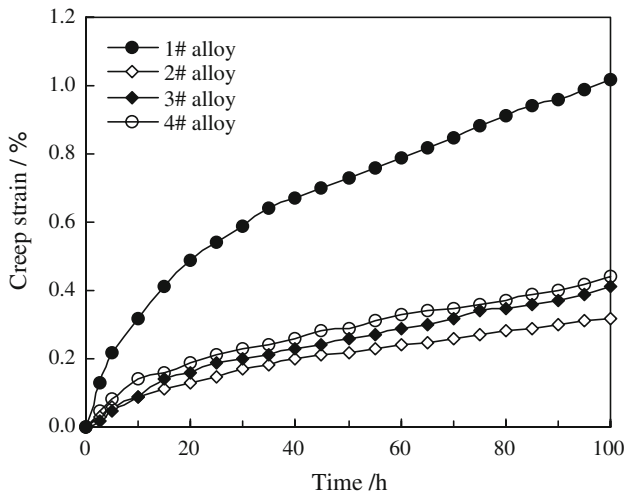

Fig. 11 Tensile creep curves of the as-cast experimental alloys at 150 °C and 50 MPa

improvement of creep properties for the Mg–3.8Zn–2.2Ca alloy by Ce, Sn and Gd additions are possibly related to the precipitation of $Mg_{12}Ce$, CaMgSn and Mg_5Gd with relatively high thermal stability, respectively. In addition, it is also observed from Fig. 11 and Table 3 that among the Ce-, Sn- and Gd-containing Mg–3.8Zn–2.2Ca alloys the creep properties of the Sn- and Gd-containing alloys are similar but lower than those of the Ce-containing alloy. The possible reason for the difference in the creep properties for the Ce-, Sn- and Gd-containing Mg–3.8Zn–2.2Ca alloys will be discussed in the following section.

Table 3 Creep properties of the as-cast experimental alloys at 150 °C and 50 MPa for 100 h

Experimental alloys	Total creep strain (%)	Minimum creep rate ($\times 10^{-8}$ s^{-1})
1# alloy	1.02	2.83
2# alloy	0.32	0.90
3# alloy	0.41	1.14
4# alloy	0.44	1.22
AE42 alloy [1]	≈0.14	≈0.39
AZ91 alloy [1]	≈0.85	≈2.36

Discussion

The above-mentioned results indicate that adding 1.0 wt% Ce, 1.0 wt% Sn and 1.0 wt% Gd can effectively refine the grains of Mg–3.8Zn–2.2Ca alloy and thus lead to an improvement of tensile properties of the alloy. Figure 12 shows the X-ray mapping results for the Ce-, Sn- and Gd-containing Mg–3.8Zn–2.2Ca alloys. It is observed that the Ce, Sn and Gd elements mainly distribute at the respective grain boundaries. Therefore, it is inferred that the above observed grain refinement of Ce-, Sn- and Gd-containing Mg–3.8Zn–2.2Ca alloys is possibly related to the Ce, Sn and Gd enrichment of the liquid during solidification, which induces a constitution undercooling at the solidification interface front, thus accelerating the growth of secondary dendrites and refining the grains. In addition, it is reported [18–20] that the $Mg_{12}Ce$, CaMgSn and Mg_5Gd

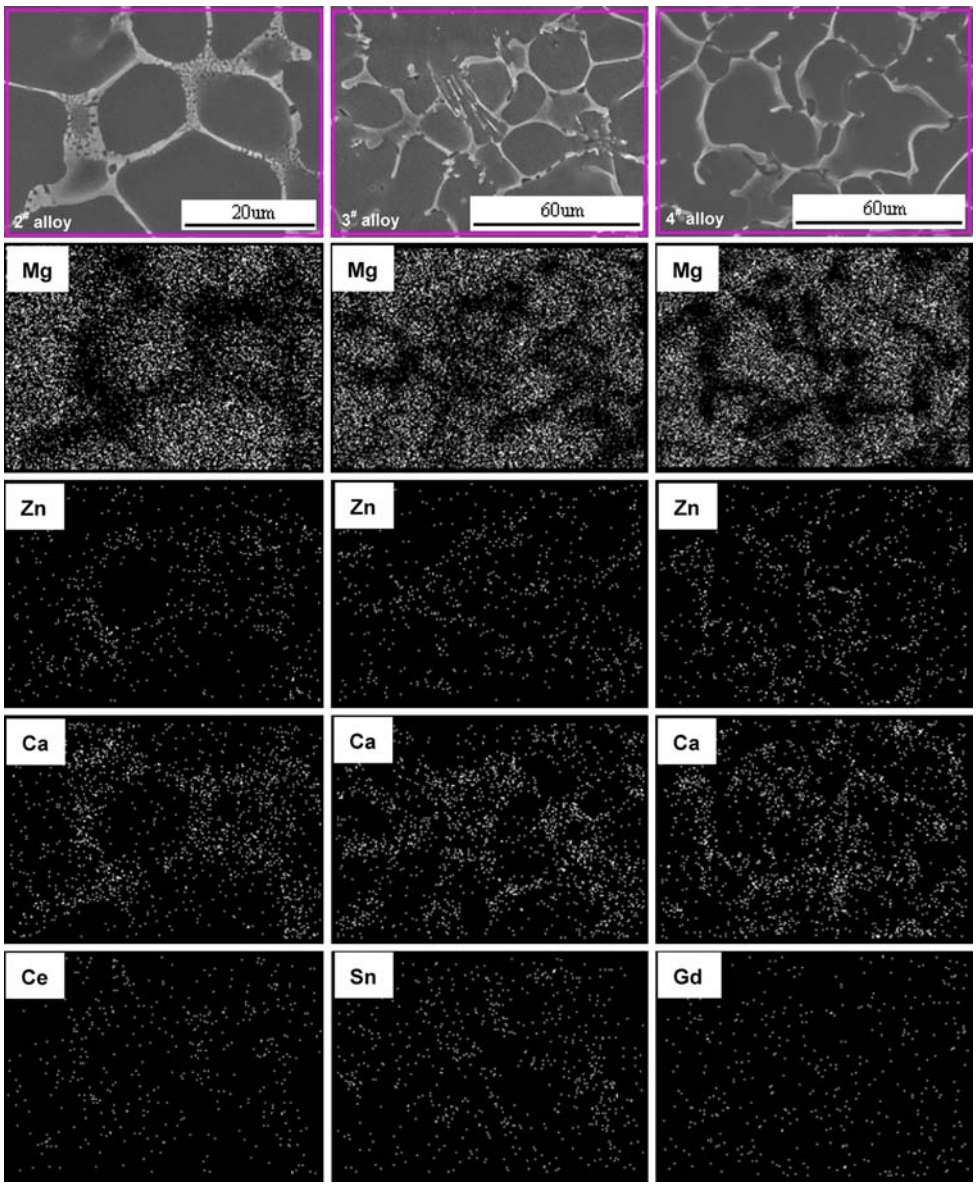

Fig. 12 X-ray mapping results for the 2–4# as-cast experimental alloys

compounds, which have high melting points and heat resistance, can restrain the growth of α-Mg at the high temperatures, consequently the grains are further refined. In spite of the above-mentioned analysis, the reason for the observed difference of Ce, Sn and Gd addition in the grain refinement of Mg–3.8Zn–2.2Ca alloy is not clear. Further investigation still needs to be considered.

In addition, the above-mentioned results also indicate that the creep properties of the Ce-, Sn- and Gd-containing Mg–3.8Zn–2.2Ca alloys are different. The creep properties of the Sn- and Gd-containing alloys are similar but lower than that of the Ce-containing alloy. The reason for the difference in the creep properties is possibly related to the variation in microstructural features. One significant microstructural factor is grain size. It is generally accepted that the rate of dislocation creep tends to decrease with increasing grain size due to a lowered contribution of grain boundary sliding [30]. Since the grain size of the Ce- and Sn-containing alloys is similar and relatively smaller than that of the Gd-containing alloy, the grain size effect cannot explain the difference in the creep properties. Obviously, the difference in the creep properties is possibly related to other factors. It is well known that the increase in creep resistance of Mg–Al based alloys containing rare earths is caused by the suppression of the formation of the $Mg_{17}Al_{12}$ phase which tends to be unstable at elevated temperature, and there is also the solid solution strengthening and precipitates that can pin grain boundaries to prevent grain boundary sliding [1]. As shown in Fig. 7, there is an obvious difference in the morphology of the eutectic particles for the Ce-, Sn- and Gd-containing Mg–3.8Zn–2.2Ca alloys. The eutectic particles of Ce-containing alloy are a

more intimate mixture while the eutectic particles of the Sn- and Gd-containing alloys are a continuous divorced structure. Therefore, it is inferred that the difference in the creep properties for the Ce-, Sn- and Gd-containing Mg–3.8Zn–2.2Ca alloys is possibly related to the strengthening effect of eutectic particles.

Although the above-mentioned results indicate that adding 1.0 wt% Ce, 1.0 wt% Sn and 1.0 wt% Gd to the Mg–3.8Zn–2.2Ca alloy can effectively improve the tensile and creep properties of the as cast alloy, a question remains as to whether these additions influence the age-hardening response of the alloy, since the ternary composition belongs to a typical age hardenable system. Therefore, further research is also needed to optimize the amount of Ce, Sn and Gd additions and understand their effects on the tensile and creep properties and age-hardening behavior of the Mg–3.8Zn–2.2Ca alloy.

Conclusions

(1) Adding 1.0 wt% Ce, 1.0 wt% Sn or 1.0 wt% Gd can effectively refine the grains of the Mg–3.8Zn–2.2Ca alloy, and the refinement efficiency of Ce addition is relatively high, followed by the additions of Sn and Gd, respectively. Accordingly, the tensile properties of the as-cast Mg–3.8Zn–2.2Ca alloy are improved by the additions of Ce, Sn or Gd, with the improvement resulting from the Ce addition being best and followed by the additions of Sn and Gd, respectively.

(2) Adding 1.0 wt% Ce, 1.0 wt% Sn or 1.0 wt% Gd to the Mg–3.8Zn–2.2Ca alloy can improve the creep properties of the as-cast alloy. Among the Ce-, Sn- and Gd-containing alloys the creep properties of the Sn- and Gd-containing alloys are similar but lower than that of the Ce-containing alloy. The difference in the creep properties for the Ce-, Sn- and Gd-containing alloys is possibly related to the strengthening effect of eutectic particles rather than the effect of grain size.

Acknowledgements The present work was supported by the National Natural Science Funds in China (No. 50725413), the Major State Basic Research Development Program of China (973) (No. 2007CB613704), the Natural Science Foundation Project of CQ CSTC (No. 2007BB4400), and the Chongqing Education Commission in China (KJ090628).

References

1. Luo A, Pekguleryuz MO (1994) J Mater Sci 29:5259. doi:10.1007/BF01171534
2. Bamberger M, Dehm G (2008) Annu Rev Mater Res 38:505
3. Gorny A, Bamberger M, Katsman A (2007) J Mater Sci 42:10014. doi:10.1007/s10853-007-1998-7
4. Levi G, Avraham S, Zilberov A, Bamberger M (2006) Acta Mater 54:523
5. Bettles CJ, Gibson MA, Venkatesan K (2004) Scr Mater 51:193
6. Nie JF, Muddle BC (1997) Scr Mater 37:1475
7. Chang S-Y, Fukatsu A, Tezuka H, Kamio A (1999) Mater Trans 40:546
8. Oh JC, Ohkubo T, Mukai T, Hono K (2005) Scr Mater 53:675
9. Horie T, Iwahori H, Awano Y, Matsui A (1999) J Jpn Inst Light Met 49:272
10. Mendis CL, Oh-ishi K, Hono K (2007) Scr Mater 57:485
11. Gao X, Zhu SM, Muddle BC, Nie JF (2005) Scr Mater 53:1321
12. Somekawa H, Mukai T (2007) Mater Sci Eng A 459:366
13. Ortega Y, Leguey T, Pareja R (2008) Mater Lett 62:3893
14. Zhou T, Chen D, Chen ZH, Chen JH (2009) J Alloys Compd 475:L1
15. Chen ZH, Zhou T, Chen D, Yan HG, Chen JH (2008) Mater Sci Technol 24:848
16. Jardim PM, Solorzano G, Vander Sande JB (2004) Mater Sci Eng A 381:196
17. Park WW, You BS, Moon BG, Park JG, Yang SC (2001) Met Mater Int 7:9
18. Yang MB, Pan FS, Cheng L, Shen J (2009) Mater Sci Eng A 512:132
19. Chen JH, Chen ZH, Yan HG, Zhang FQ, Liao K (2008) J Alloys Compd 461:209
20. He SM, Peng LM, Zeng XQ, Ding WJ, Zhu YP (2006) Mater Sci Eng A 433:175
21. Zhou HT, Zeng XQ, Liu LF, Zhang Y, Zhu YP, Ding WJ (2004) J Mater Sci 39:7061. doi:10.1023/B:JMSC.0000047551.04037.fe
22. Jun JH, Kim JM, Park BK, Kim KT, Jung WJ (2005) J Mater Sci 40:2659. doi:10.1007/s10853-005-2099-0
23. Mishra RK, Gupta AK, Rao PR, Sachdev AK, Kumard AM, Luo AA (2008) Scr Mater 59:562
24. Moreno IP, Nandy TK, Jones JW, Allison JE, Pollock TM (2001) Scr Mater 45:1423
25. Qian Ma, Das A (2006) Scr Mater 54:881
26. Brubaker CO, Liu Z-K (2004) J Alloys Compd 370:114
27. Zhang EL, Yang L (2008) Mater Sci Eng A 497:111
28. Hort N, Huang Y, Abuleil T, Maier P, Kainer KU (2006) Adv Eng Mater 8:359
29. Kim BH, Jeon JJ, Park KC, Park BG, Park YH, Park IM (2008) Int J Cast Met Res 21:186
30. Zhu SM, Mordike BL, Nie JF (2008) Mater Sci Eng A 483–484:583